Compressible ferrimagnetism in the depleted periodic Anderson model

N. C. Costa, M. V. Araújo, J. P. Lima, T. Paiva, R. R. dos Santos, and R. T. Scalettar

Compressible Ferrimagnetism in the depleted Periodic Anderson Model

N.C. Costa,[1, 2] M.V. Araújo,[3] J.P. Lima,[3] T. Paiva,[1] R.R. dos Santos,[1] and R.T. Scalettar[2]

[1]*Instituto de Física, Universidade Federal do Rio de Janeiro Cx.P. 68.528, 21941-972 Rio de Janeiro RJ, Brazil*
[2]*Department of Physics, University of California, Davis, CA 95616, USA*
[3]*Departamento de Física, Universidade Federal do Piauí, Teresina PI, Brazil*

Tight-binding Hamiltonians with single and multiple orbitals exhibit an intriguing array of magnetic phase transitions. In most cases the spin ordered phases are insulating, while the disordered phases may be either metallic or insulating. In this paper we report a Determinant Quantum Monte Carlo study of interacting electrons in a geometry which can be regarded as a two-dimensional Periodic Anderson Model with depleted interacting (f) orbitals. For a single depletion, we observe an enhancement of antiferromagnetic correlations and formation of localized states. For half of the f-orbitals regularly depleted, the system exhibits a ferrimagnetic ground state. We obtain a quantitative determination of the nature of magnetic order, which we discuss in the context of Tsunetsugu's theorem, and show that, although the dc conductivity indicates insulating behavior at half-filling, the compressibility remains finite.

I. INTRODUCTION

Tight binding Hamiltonians provide insight into many of the properties of strongly correlated electron systems, from magnetism and metal-insulator transitions, to superconductivity and charge ordering[1,2]. The simplest of these, the single band Hubbard model (HM), is known, for example, to be insulating and to exhibit long range antiferromagnetic (AF) order at half-filling on a square lattice[3,4] for any ratio of the on-site interaction U to hopping t, and to undergo a paramagnetic metal to insulating AF transition above a nonzero critical U_c on other geometries such as the honeycomb lattice. The Nagaoka theorem[5], notwithstanding the ferromagnetic behavior, which is robust within mean-field theory[2,3], seems to be difficult to achieve when the single band Hamiltonian is solved with more exact methods[6].

The generalization of tight-binding Hamiltonians to multiple bands opens up a richer variety of magnetic behavior. In the case of the periodic Anderson model (PAM), the interplay of the on-site repulsion U_f on localized (f) orbitals with the hybridization V to a noninteracting conduction (d) band results in a competition of long range magnetic order arising from the Ruderman-Kittel-Kasuya-Yosida (RKKY) interaction (at small V) and spin liquid behavior (at large V).[7–10] Not uncommonly in these more complex situations, orbital ordering coexists with spin ordering[11].

Many of these models offer quite remarkable insights into strongly correlated materials; for instance, the HM replicates several prominent qualitative features of cuprate superconductors, such as the AF and d-wave pairing, as well as stripe formation.[12–17] The AF-singlet transition and strongly renormalized effective electronic mass in the PAM, and its strong coupling limit (the Kondo lattice model) helps to explain different ground states in heavy-fermion materials.[8,18–22] Manganites[23] and iron-pnictide superconductors[24] are also materials for which appropriate multi-orbital models have been useful for developing an understanding of magnetism, pairing, charge order, and transport.

Geometries which can be regarded as arising from regular 'depletions' of the square lattice HM have also been explored, both to answer fundamental questions about types of magnetic order and for the understanding of specific materials. An example of the former is Lieb's theorem[25], which rigorously demonstrates that a 1/4-depleted square lattice possesses ground state ferrimagnetic behavior. Instances of the latter are the 1/5-depleted square lattice which can explain spin liquid behavior in CaV_4O_9[26,27], and the 1/3-depleted square lattice which shed light into the properties of layered nickelates such as $La_4Ni_3O_8$[28–30]. In these situations, the depletion converts the initial single band nature to a model with multiple bands. In the case of the Lieb lattice, one of these bands is dispersionless, a feature which is intimately tied to the appearance of ferromagnetism. (Random) site depletion of tight-binding Hamiltonians has also been used to understand the effects of the substitution of nonmagnetic atoms for magnetic ones, for example the replacement of Cu by Zn in cuprate materials.[31–34] In cases where the underlying geometry contains triangular lattice coordination, depletion can aid AF behavior by reducing frustration,[35] e.g. in $CeAl_3$. More complex cases, such as depletion in the PAM seems relevant to understand the formation of magnetism in heavy fermion materials. In this case, mean-field and perturbation theory[36–40] have provided evidence of a ferromagnetic ground state.

In view of this, we investigate the combination of these two avenues, a PAM which *begins* already with two bands, but is then subject to site depletion. Our main conclusion is that depletion can drive the PAM into a magnetically ordered state, even for parameter choices which are deep in the singlet phase for the undepleted lattice. In addition to obtaining its magnetic phase diagram quantitatively, we will show that an unusual property develops in which the ordered regime is also compressible.

The organization of this paper is as follows: In Sec. II we define the tight-binding Hamiltonian precisely, review the Determinant Quantum Monte Carlo (DQMC) methodology[41] briefly, and define the observables used to characterize the model's properties. Section III presents data on the effect of the removal of a single site; the resulting enhanced spin response provides an initial clue to the robustness of magnetism in the regularly depleted geometry, described in Sec. IV. Section V analyzes data for the compressibility, effective hopping, and conductivity, and Sec. VI contains our conclusions.

II. MODEL

The depleted PAM we consider here is described by the Hamiltonian

$$
\begin{aligned}
\hat{\mathcal{H}} = & -t \sum_{\langle \mathbf{i},\mathbf{j}\rangle,\sigma} \left(d_{\mathbf{i}\sigma}^{\dagger} d_{\mathbf{j}\sigma} + \text{h.c.} \right) - V \sum_{\mathbf{i}\sigma}' \left(d_{\mathbf{i}\sigma}^{\dagger} f_{\mathbf{i}\sigma} + \text{h.c.} \right) \\
& + U_f \sum_{\mathbf{i}}' \left(n_{\mathbf{i}\uparrow}^{f} - \frac{1}{2} \right) \left(n_{\mathbf{i}\downarrow}^{f} - \frac{1}{2} \right) \\
& + \sum_{\mathbf{i}\sigma} \epsilon_{\mathbf{i}}^{d} d_{\mathbf{i}\sigma}^{\dagger} d_{\mathbf{i}\sigma} + \sum_{\mathbf{i}\sigma}' \epsilon_{\mathbf{i}}^{f} f_{\mathbf{i}\sigma}^{\dagger} f_{\mathbf{i}\sigma} \\
& - \mu \sum_{\mathbf{i}\sigma} d_{\mathbf{i}\sigma}^{\dagger} d_{\mathbf{i}\sigma} - \mu \sum_{\mathbf{i}\sigma}' f_{\mathbf{i}\sigma}^{\dagger} f_{\mathbf{i}\sigma},
\end{aligned}
\tag{1}
$$

where the unprimed sums over $\mathbf{i}$ run over a two dimensional square lattice, with $\langle \mathbf{i},\mathbf{j}\rangle$ denoting nearest-neighbors, while the primed sums are restricted to the set of sites having f-orbitals. The specific depletion patterns will be described in the coming sections. The first term on the right-hand side of Eq. (1) represents the hopping of d-electrons, while the second term contains the hybridization, V, between d and f-orbitals. The Coulomb repulsion on localized f-orbitals is included in the third term, with $n_{\mathbf{i}\sigma}^{f} = f_{\mathbf{i}\sigma}^{\dagger} f_{\mathbf{i}\sigma}$ being the number operator of f-electrons. The last two terms correspond to onsite energies $\epsilon_{\mathbf{i}}^{d}$ and $\epsilon_{\mathbf{i}}^{f}$ of d and f-orbitals, respectively. The hopping integral $t \equiv 1$ defines the scale of energy.

We analyze Eq. (1) using the DQMC method, a numerically exact technique in which all sources of error, statistical (from finite sampling times) and systematic (from the discretization of the inverse temperature β) can be removed to the desired degree of accuracy. The basic idea of the method is the use of the Trotter-Suzuki decomposition to separate the exponentials of the one-body and two-body pieces, $\hat{\mathcal{K}}$ and $\hat{\mathcal{P}}$ respectively, in the partition function, $\mathcal{Z} = \text{Tr}\, e^{-\beta\hat{\mathcal{H}}} = \text{Tr}\left[\left(e^{-\Delta\tau(\hat{\mathcal{K}}+\hat{\mathcal{P}})} \right)^{l} \right] \approx \text{Tr}\left[e^{-\Delta\tau\hat{\mathcal{K}}} e^{-\Delta\tau\hat{\mathcal{P}}} e^{-\Delta\tau\hat{\mathcal{K}}} e^{-\Delta\tau\hat{\mathcal{P}}} \cdots \right]$. Here $l = \beta/\Delta\tau$ is the number of incremental time evolution operators. This decomposition has an error proportional to $(\Delta\tau)^2$ and is exact in the limit $\Delta\tau \to 0$. The resulting isolation of $e^{-\Delta\tau\hat{\mathcal{P}}}$ allows for the performance of a discrete Hubbard-Stratonovich (HS) transformation so that it can be rewritten in quadratic (single body) form, but with

the cost of introducing a discrete auxiliary field with components on each of the space and imaginary time lattice coordinates. The fermions are then integrated out, and the HS field is sampled by the Monte Carlo technique. In the work we report here we choose $t\Delta\tau = 0.125$ so that the error from the Trotter-Suzuki decomposition is less than, or comparable to, that from the Monte Carlo sampling. We therefore report error bars from the latter. More details about the method are discussed in Ref. 42 and references therein.

Although DQMC is exact, its low temperature application is restricted to systems with particle-hole or other symmetries[43], owing to the minus-sign problem[44,45]. For this reason, our focus is on half-filling, $\mu = \epsilon^f = \epsilon^d = 0$, where the sign problem is absent. Fortunately, this density is of considerable interest, both because of the strong magnetic order favored by commensurate filling, and by the materials for which half-filling is appropriate (e.g. the undoped parent compounds of the cuprate superconductors). Depleting f-orbitals, i.e. removing them from the lattice, preserves particle-hole symmetry (PHS). This is true regardless of the number or pattern of the removed sites, in much the same way that PHS is present for arbitrary (including position-dependent) choices of the energy scales t, V, and U_f, as long as the hopping only connects sites on opposite sublattices of a bipartite lattice.

We concentrate on the following observables: The magnetic features of the Hamiltonian will be characterized by the real space spin-spin correlation function,

$$
C^{\alpha\gamma}(\mathbf{j}) = \langle S_{\mathbf{j_o}+\mathbf{j}}^{\alpha,-} S_{\mathbf{j_o}}^{\gamma,+} \rangle = \langle c_{\mathbf{j_o}+\mathbf{j}\downarrow}^{\alpha\,\dagger} c_{\mathbf{j_o}+\mathbf{j}\uparrow}^{\alpha} c_{\mathbf{j_o}\uparrow}^{\gamma\,\dagger} c_{\mathbf{j_o}\downarrow}^{\gamma} \rangle, \tag{2}
$$

where the orbital indices are $\alpha, \gamma = d, f$. (Later in the paper, we will use an alternate notation which further distinguishes the two types of conduction electron orbitals, those with a partner f orbital and those for which the partner has been removed.) As the notation suggests, $C^{\alpha\gamma}(\mathbf{j})$ is independent of $\mathbf{j_o}$ for translationally invariant geometries. The Fourier transform of $C^{\alpha\gamma}(\mathbf{j})$ is the magnetic structure factor,

$$
S^{\alpha\gamma}(\mathbf{q}) = \sum_{\mathbf{j}} C^{\alpha\gamma}(\mathbf{j})\, e^{i\mathbf{q}\cdot\mathbf{j}}. \tag{3}
$$

In addition to these equal time correlation functions, we also measure appropriate unequal-time quantities including the magnetic susceptibility,

$$
\chi^{\alpha\gamma}(\mathbf{q}) = \sum_{\mathbf{j}} \int_0^{\beta} d\tau \langle S_{\mathbf{j_o}+\mathbf{j}}^{\alpha,-}(\tau) S_{\mathbf{j_o}}^{\gamma,+}(0) \rangle\, e^{i\mathbf{q}\cdot\mathbf{j}}. \tag{4}
$$

For χ we will mostly examine the uniform case, $\mathbf{q} = 0$. Although we have defined both the equal time correlations, Eq. (2), and susceptibility, Eq. (4), in terms of the xy $(+-)$ spin components, these are, by symmetry, equivalent to those in the z direction.
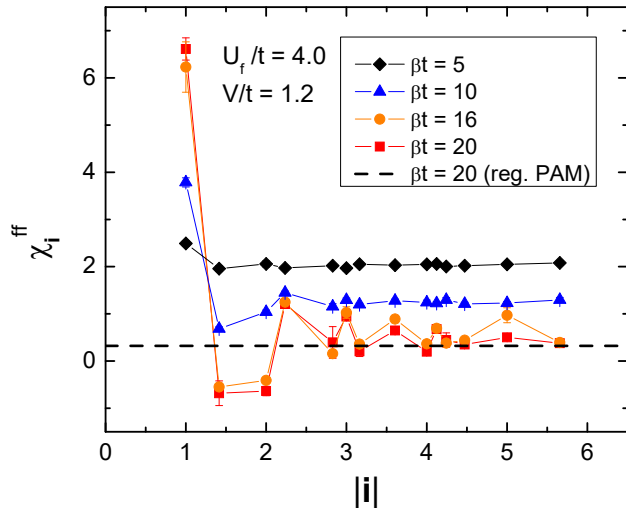
FIG. 1: (Color online) Local susceptibility of f-orbitals as a function of distance $|\mathbf{i}|$ from the ion defect. The dashed black line is the value of the magnetic susceptibility in the undepleted PAM at $\beta t = 20$. Here, and in all subsequent figures, when not shown, the error bars are smaller than the symbol size.

FIG. 2: (Color online) Contour plot of the f-orbital local susceptibilities for $\beta t = 20$. The central black square marks the geometrical position of the site where the f-orbital was depleted.

Metal-insulator transitions are characterized via the electronic compressibility (κ) and the dc conductivity (σ_{dc}). The former is defined as

$$\kappa = -\frac{1}{\rho^2}\frac{\partial \rho}{\partial \mu}, \qquad (5)$$

where ρ is the electronic density. The conductivity, σ_{dc}, is evaluated as

$$\sigma_{dc} = \frac{\beta^2}{\pi}\Lambda_{xx}(\mathbf{q} = \mathbf{0}, \tau = \beta/2), \qquad (6)$$

with

$$\Lambda_{xx}(\mathbf{q}, \tau) = \langle j_x(\mathbf{q}, \tau) j_x(-\mathbf{q}, 0)\rangle, \qquad (7)$$

where $j_x(\mathbf{q}, \tau)$ is the $\mathbf{q}$-τ dependent current in x direction, the Fourier transform of $j_x(l) = -\mathrm{i}\sum_l t_{l+\hat{x},l}(c_{l+\hat{x},\sigma}^\dagger c_{l,\sigma} - c_{l,\sigma}^\dagger c_{l+\hat{x},\sigma})$. The assumptions involved in the use of Eq. (6) to evaluate the conductivity are discussed in Refs.[46,47] and are tested there for a variety of situations. At this point it is instructive to mention that κ measures the accommodation of additional electrons (or holes) into the system, while σ_{dc} probes the effective charge transport throughout the lattice. In view of this, σ_{dc} provides a more stringent criteria for metallicity.

III. SINGLE DEPLETION

An interesting step towards understanding f-orbital depleted systems is to consider an isolated impurity. In fact, there have been a number of recent studies
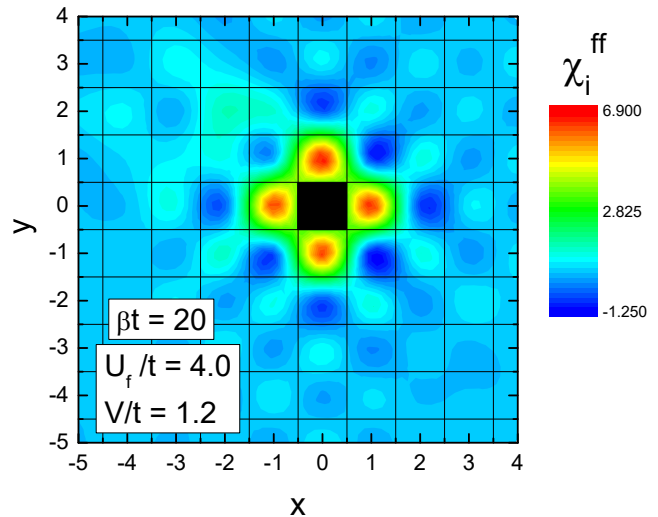
on the alteration of the magnetic structure around impurities in heavy fermion materials and their possible description within the PAM[48–54]. Hence, we first discuss how depletion of a single f-orbital affects magnetic and spectral properties, and compare with the uniform case of the undepleted PAM. Inclusion of a magnetic defect breaks translational symmetry. We therefore generalize Eq. (4) to the local magnetic susceptibility at site $\mathbf{i}$ by

$$\chi_{\mathbf{i}}^{\alpha\gamma} = \sum_{\mathbf{j}\in\gamma}\int_0^\beta d\tau \langle S_{\mathbf{i}}^{\alpha,-}(\tau)S_{\mathbf{j}}^{\gamma,+}(0)\rangle, \qquad (8)$$

where the sum runs over all sites $\mathbf{j}$ with orbital γ. The total susceptibility, Eq.(4), is the sum of these local susceptibilities. $\chi_{\mathbf{i}}^{\alpha\gamma}$ would be probed experimentally via nuclear magnetic resonance and, indeed, such site- and orbital-specific NMR has been used to explore spin and charge patterns in doped heavy fermion[49,53] and iron-pnictide superconductors[52].

We analysed a 10×10 lattice, using periodic boundary conditions, with the depleted site defining the origin of the lattice. Because one of the most interesting aspects of site removal is the possibility of enhancing magnetism[54], we fix the hybridization at $V/t = 1.2$ and the repulsive potential as $U_f/t = 4$, so that we are in the spin-singlet phase of the undepleted PAM[7,10].

Figure 1 presents the behavior of the local susceptibility, Eq. (8), of the f-orbitals as a function of the distance from the depletion site. At a high temperature, $T/t = 0.2$ ($\beta t = 5$, black diamonds), the magnetic response is large and positive, and almost homogeneous throughout the lattice. When the temperature is decreased, $T/t = 0.10 - 0.05$, the local susceptibility increases on nearest neighbor (NN) sites. This is the opposite of what happens in the conventional
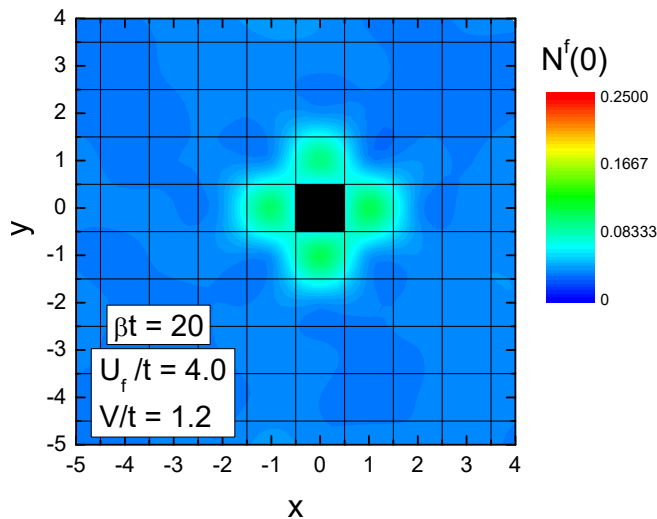
FIG. 3: (Color online) Contour plot of the local f electron density of states, $N_{\mathbf{i}}^{f}(0)$, for $\beta t = 20$. The black square corresponds to the impurity location, as in Fig. 2.

FIG. 4: (Color online) Contour plot of the conduction electron density of states, $N_{\mathbf{i}}^{c}(0)$, for $\beta t = 20$.

PAM, where, in the singlet phase at $V/t = 1.2$, the magnetic susceptibility goes to zero as a consequence of the spin gap in the ground state. Indeed, at $\beta t = 20$ (red squares), the NN magnetic susceptibility is an order of magnitude larger than the undepleted PAM (dashed black line).

On the other hand, as T is lowered, the next-nearest neighbors (NNN) of the defect exhibit a lower, but negative, magnetic response, providing evidence of antiferromagnetic correlations around the depleted site. As the distance from the depleted site grows, $\chi_{\mathbf{i}}^{ff}$ decays with distance, eventually approaching the value for the regular PAM. An alternate visualization of the enhancement of antiferromagnetic correlations, is given in Fig. 2, a color contour plot of $\chi_{\mathbf{i}}^{ff}$. The formation of a small antiferromagnetic 'cloud' around the magnetic defect is evident. When the hybridization is increased (not shown) the magnetic response for the NN sites remains high, but is strongly suppressed on sites farther from the impurity. The characteristic size of the 'cloud' decreases as one moves deeper into the singlet phase. The results of Figs. 1 and 2 are consistent with DMRG calculations for a single depletion in the one-dimensional Kondo Lattice Model (KLM)[55] and with the behavior of a corresponding model of localized spins; see Ref. 54.

As noted earlier, the presence of magnetic clouds around impurities is a characteristic feature of real materials. In the heavy fermion $CeCo(In_{1-x}Cd_x)_5$, for example, an antiferromagnetic region appears around Cd impurities, with a size that can be tuned with pressure[48–51]. The Cd substitution contributes with a delocalized p-orbital,[79] thereby locally changing the hybridization and breaking up the local singlet; the net effect is the appearance of an effective local moment at the impurity site, which interacts with its neighbors.[50,51]
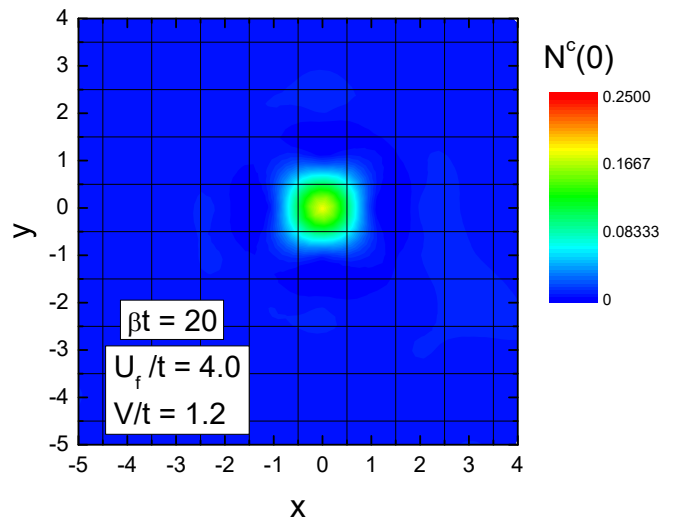
In this particular situation, a model more appropriate than that of Eq. (1) is one in which the moment on an impurity site has an altered hybridization V to the conduction electrons[53]. However, magnetic domains around sites in which the moment is removed have also been studied[56–58].[80]

The preceding result is suggestive of the breaking of the local singlet state, an effect we will see in even more dramatic form when a collection of f sites is removed. It is also worth examining the spectral properties of the system. We compute the local density of states (DOS) by analytic continuation of the imaginary-time dependent Green's function, inverting the integral equation

$$G_{\mathbf{i}}(\mathbf{j} = 0, \tau) = \int \mathrm{d}\omega\, N_{\mathbf{i}}(\omega)\, \frac{e^{-\omega\tau}}{e^{\beta\omega} + 1}, \qquad (9)$$

where $\mathbf{i}$ denotes the site position, while $\mathbf{j}$ is the displacement between sites where the creation and annihilation operators of the Green's function are applied. As discussed in Ref. 59, for low temperatures the DOS at $\omega = 0$ can be written as

$$N_{\mathbf{i}}(\omega = 0) \approx -\beta G_{\mathbf{i}}(\mathbf{j} = 0, \tau = \beta/2)/\pi. \qquad (10)$$

In Fig. 3 we present a contour plot for $N_{\mathbf{i}}^{f}(0)$ at $\beta t = 20$. At sites far from the magnetic defect, the local DOS vanishes, as expected in the spin-singlet phase. Near the impurity, there is a large DOS, supporting the picture of broken singlets around the defect, in accordance with the local magnetic susceptibility results, discussed above. As displayed in the contour plot of Fig. 4, precisely at the impurity site the conduction electron DOS, $N_{\mathbf{i}}^{c}(0)$, is large, owing to the absence of a partner f electron.

To provide an independent check on the validity of Eq. (10), we performed a direct inversion of Eq. (9), using the Maximum Entropy Method[60]. The local DOS is
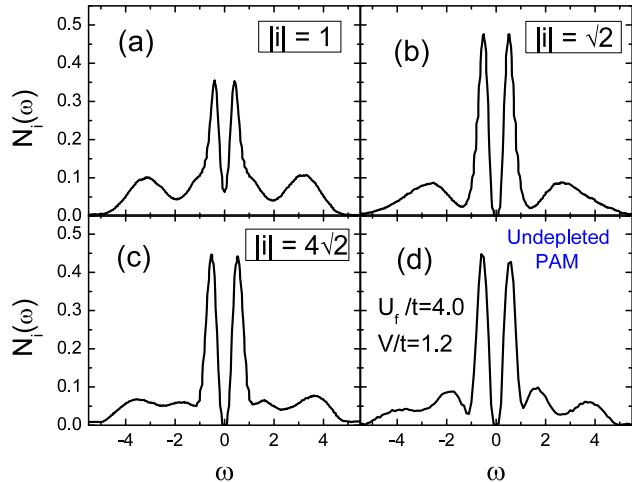
FIG. 5: DOS of sites at distance (a) $|\mathbf{i}| = 1$, (b) $\sqrt{2}$ and (c) $4\sqrt{2}$ from the depleted site, as well as (d) the regular (undepleted) PAM, both for $\beta t = 20$ and $V/t = 1.20$. At short distances, the singlet gap present in the undepleted PAM is partially filled in, so that there is nonvanishing f spectral weight at $\omega = 0$.

FIG. 6: (Color online) (a) The lattice geometry for the regularly half depleted PAM. The unit cell is composed by the sites d_0, d_1 and f. Here we depict a lattice with $N_{cells} = 2 \times 2^2$. (b) The band structure in the noninteracting case for $V \neq 0$.

displayed in Fig. 5 for sites at (a) $|\mathbf{i}| = 1$ (nearest neighbors), (b) $\sqrt{2}$ (next-nearest neighbors) and (c) $4\sqrt{2}$ far from the magnetic defect. As in Figs. 3 and 4, we fixed $\beta t = 20$. We also present in Fig. 5 (d) the DOS of the undepleted PAM, at the same temperature and hybridization. Notice that for $V/t = 1.20$, the undepleted PAM is in the spin-singlet phase and has a gap in the DOS. Although the charge gap of the homogeneous system is recovered at large $|\mathbf{i}|$, the results suggest that a single depletion in the spin singlet phase of the PAM creates non-vanishing spectral weight in the f-sites around the defect (and a localized state in the unpaired d orbital). Similar analyses within a mean-field approach were performed in Refs. 61 and 62, where a gain is also observed in spectral weight owing to f-orbital depletion.

To summarize: our results provide evidence of enhancement of short range magnetic correlations and local density of states, which we interpret as arising from the breaking of spin singlets near the impurity[54,55,63,64]. We now turn to the main theme of this manuscript, namely what happens with a regular collection of depleted sites, and specifically, whether the local magnetic regions coalesce into long range order. Such problems were first addressed in Refs. 65 and 66 for the PAM and KLM, respectively, within a mean-field approach. Recent mean-field results for the PAM, presented in Ref. 36, also provide evidence of a ferromagnetic ground state. Similarly, unbiased methods for an analogous spin model, namely the bilayer Heisenberg model (Ref. 54), shows that, indeed, the depletion of spins induces an AFM ground state. As
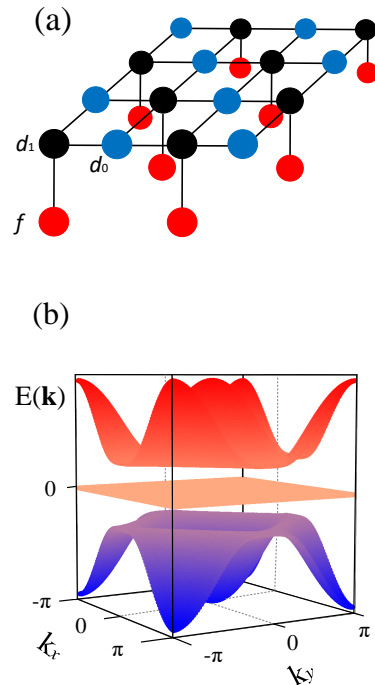
we shall see in the next Section, magnetic long range order indeed occurs, even deep in what was previously the singlet phase of the undepleted model (large d-f hybridization). However, as presented below, the system still has a "memory" of the old critical point.

IV. HALF DEPLETION

Our previous results suggest that if the number of nonmagnetic defects increases, the magnetic correlations can be enhanced, and thus the ground state may exhibit magnetic long range order even if the undepleted model is in the singlet phase. Here we explore the case of depletion of half of the f-orbitals, in the checkerboard pattern of Fig. 6. The possibility of a magnetic ground state in such a geometry is supported by exact results, such as Tsunetsugu's theorem[67] for the KLM, and Lieb's theorem for the Hubbard model[25,68,69]. The former is particularly relevant in the present case, owing to the close relationship between the PAM and the KLM. Tsunetsugu showed that the ground state of the KLM on a bipartite lattice and at half filling has total spin $S = |N_\mathcal{A} - N_\mathcal{B}|/2$, where $N_\mathcal{A}$ and $N_\mathcal{B}$ are the number of sites in sublattices $\mathcal{A}$ and $\mathcal{B}$, respectively. In this theorem, the localized spins are also included when
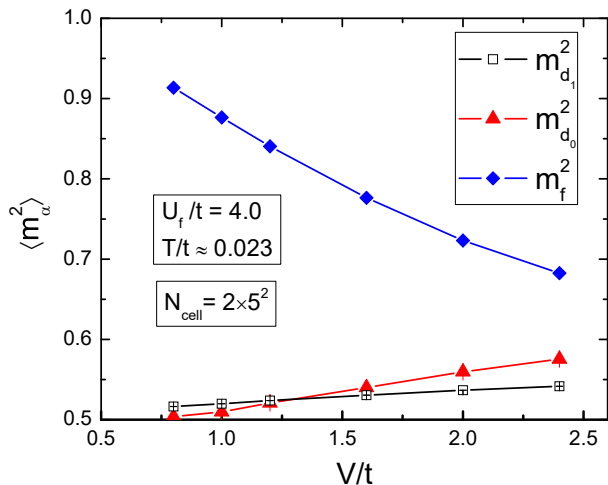
FIG. 7: (Color online) Local moments on the three types of sites as functions of hybridization at a low temperature.

counting the number of sites on each sublattice, with their labels (i.e. belonging to $\mathcal{A}$ or $\mathcal{B}$) depending on the sign of the Kondo interaction. There is no assumption of translational symmetry in this result: missing sites can be randomly located. Although this theorem was proved for the KLM, one might expect a similar behavior in the closely-related PAM. If so, the total spin of the PAM in the half depleted lattice of Fig. 6 should be finite, i.e. a ferromagnetic ground state. Our goal here is to confirm this conjecture within unbiased methods, and, more importantly, to quantify the details of the individual orbital contributions to magnetism as a function of the hybridization between the conduction and localized electrons, which is beyond the scope of the theorem.

Let us first introduce a notation which simplifies the identification of different sites/orbitals. Since we depleted all f-orbitals from one sublattice, we have two different types of d-orbitals, d_0 and d_1: the former (latter) corresponds to d-orbitals without (with) hybridization with f-orbitals, as displayed in Fig. 6. In addition, the unit cell for this geometry is composed of three sites, one of each type, with unit vectors $\mathbf{a}_1 = a(1,1)$ and $\mathbf{a}_2 = a(1,-1)$. Here a is the distance between nearest d_0 and d_1 sites. We choose $a = 0.5$ so that the distance between neighboring d_0 (or d_1) sites is 1. Finally, for technical reasons we performed our simulations on an $L \times L$ square geometry, with the primitive cell having twice the size of the unit cell, i.e. containing six sites; thus the number of unit cells is $N_{cells} = 2 \times L^2$.

We start by summarizing the noninteracting band structure: the three-site unit cell gives rise to three energy bands, with the middle one being flat (dispersionless), as is also the case for the Lieb lattice. However, unlike the Lieb lattice for which the flat band touches the dispersing bands above and below it, here the middle band is disconnected from the lower and upper bands for any positive value of the d-f hybridization
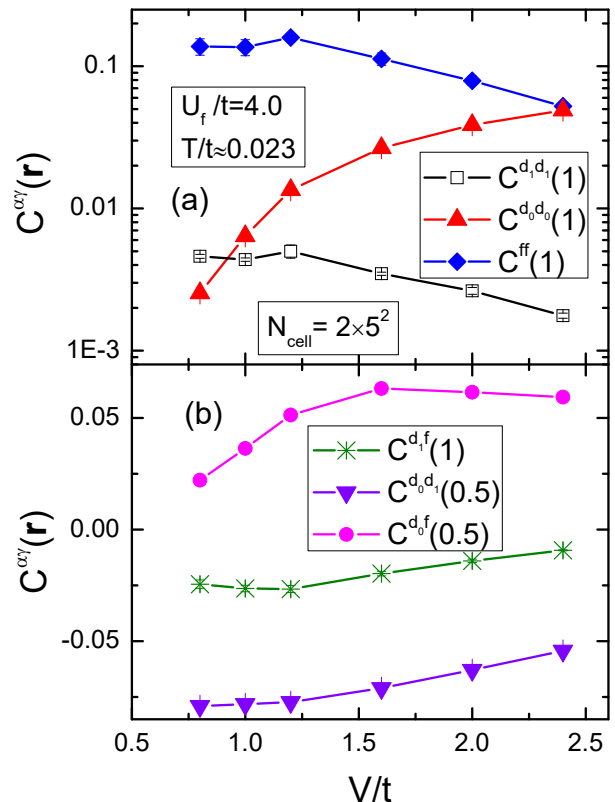

FIG. 8: (Color online) Spin-spin correlation functions for nearest pair of sites in the x-(or y-) direction: (a) $c^{d_1 d_1}(1)$, $c^{d_0 d_0}(1)$, $c^{ff}(1)$, (b) $c^{d_0 d_1}(0.5)$, $c^{d_1 f}(1)$ and $c^{d_0 f}(0.5)$. Only correlations between pairs of sites on different sublattices, that is $d_0 d_1$ and $d_1 f$, are negative (AF).

V, as displayed in Fig. 6 (b); an analogous instance for the case of a honeycomb lattice is illustrated in Ref. 39. As V increases, the gap between the middle and upper/lower bands widens, though without changing the dispersionless character of the middle band. Then, the system is a band insulator at one-third and two-thirds filling. Nevertheless, at half-filling, which is our focus here, it is similar to the Lieb case, with a partially filled flat band which, as we shall see, gives rise to bulk ferromagnetism when interactions are turned on[70].

We fix $U_f/t = 4$ and vary the strength of the f-d hybridization V/t. Figure 7 shows the local moments, $\langle (\hat{m}_\mathbf{i}^z)^2 \rangle = \langle (\hat{n}_{\mathbf{i}\uparrow} - \hat{n}_{\mathbf{i}\downarrow})^2 \rangle$ on different types of sites. When $V/t \sim 0.8$, within the AF phase of the undepleted PAM, $\langle m_f^2 \rangle$ (i.e. the local moment of the undeleted f-sites) is large, due to the suppression of the double occupancy $\langle n_\uparrow n_\downarrow \rangle$ by $U_f \neq 0$. By contrast, the conduction electron moments $\langle m_{d_0}^2 \rangle$ and $\langle m_{d_1}^2 \rangle$ are close to the half-filled non-interacting value $\langle m^2 \rangle = \langle n_\uparrow + n_\downarrow \rangle - 2\langle n_\uparrow n_\downarrow \rangle = \langle n_\uparrow + n_\downarrow \rangle - 2\langle n_\uparrow \rangle \langle n_\downarrow \rangle = 1/2$. As V increases, the hybridization between d_1 and f-sites leads to a reduction in $\langle m_f^2 \rangle$. The local moment of the d_0-sites increases with V/t much more than that of the d_1-sites, which
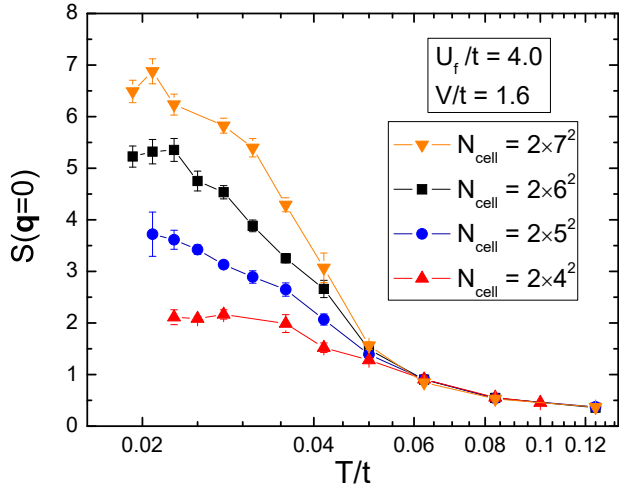
FIG. 9: (Color online) Homogeneous spin structure factor $S(\mathbf{q} = 0)$ versus temperature for $V/t = 1.6$ and $U_f/t = 4.0$.

FIG. 10: (Color online) Finite-size scaling of the total ferromagnetic structure factor. A nonzero extrpolation to $N_{cell}^{-1/2} \to 0$ indicates the presence of long range order for all the V/t values shown. Finite size corrections are largest for small V/t and for large V/t; the effective exchange coupling J_{eff} becomes small in both limits. See text.

remains roughly constant. This is somewhat surprising since V connects d_1-sites directly to f-sites, but does not hybridize the d_0 sites at all, and, more importantly, d-sites have $U = 0$. A similar behavior was recently observed[71] in the Hubbard model on a 2D superlattice with alternating rows of correlated and uncorrelated sites of different widths.

Further insight into the magnetic properties of the system can be gained by investigating non-local properties of the real space spin-spin correlation function, Eq. (2). We present, in Fig. 8, $C^{\alpha\gamma}(\mathbf{r})$ for nearest pairs of sites along the x (or y) direction, as a function of the hybridization V/t. The sign of the correlations $C^{\alpha\gamma}(\mathbf{r})$ is always positive for $\{\alpha\gamma\}=\{d_0 d_0\}$, $\{d_1 d_1\}$, $\{ff\}$ and $\{d_0 f\}$, and negative for $\{d_0 d_1\}$ and $\{d_1 f\}$ even at larger r (not shown). This is consistent with Shen's theorem[72] for the KLM, which asserts that, on bipartite lattices, $C^{\alpha\gamma}(\mathbf{r})$ is always positive for sites on the same sublattice, and always negative for sites on different sublattices.

In the undepleted case, short range spin correlations decline in magnitude upon crossing the AF-singlet quantum critical point at $V_c \sim t$; e.g., see Ref. 10. Figure 8, which resolves the spin correlations by orbital type, is useful in isolating the origin of the long range order which we will show to exist later in this Section. In particular, as seen in the figure, some of the short range correlations grow as V/t increases, contrary to the behavior in the regular PAM. For small hybridization, $C^{ff}(1)$ dominates the other correlations; it is almost two orders of magnitude larger than $C^{d_0 d_0}(1)$, for example. However, $C^{d_0 d_0}(1)$ is strongly enhanced as V/t increases, while $C^{ff}(1)$ decreases. By the time $V/t \sim 2.4$ they are roughly equal. Meanwhile, $C^{d_1 d_1}(1)$ remains small for all V. These results suggest that d_0-sites play an important role in the magnetic correlations in the ground state. Fig. 8 also indicates that antiferromagnetic correlations are present between neighboring d_0 and d_1-
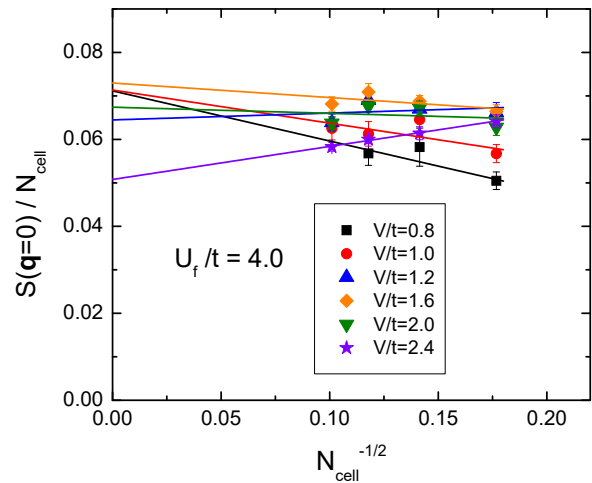
sites $[C^{d_0 d_1}(0.5)]$, and d_1 and f-sites $[C^{d_1 f}(1)]$: these decrease slowly with V. Finally, $C^{d_0 f}(0.5)$ exhibits a large and almost constant value, indicating it too contributes substantially to ground state magnetism.

According to Eq. (3), the total ferromagnetic spin structure factor normalized by the number of sites is defined as $S(0) = \frac{1}{3} \sum_{\alpha\gamma} S_{\alpha\gamma}$, with

$$S_{\alpha\gamma} = \frac{1}{N_{cells}} \sum_{\mathbf{ij}} \langle S_{\mathbf{i}}^{z(\alpha)} S_{\mathbf{j}}^{z(\gamma)} \rangle. \qquad (11)$$

As before, α and γ label the sites d_0, d_1 and f, and the sums over $\mathbf{i}$ and $\mathbf{j}$ are restricted to their positions. Fig. 9 displays the behavior of $S(0)$ at fixed $V/t = 1.6$ for different lattice sizes. At high temperatures, where spin correlations are short ranged, this quantity is independent of the size, N, of the system. However, when the ground state exhibits long range order, the sum over all sites in Eq. (3) becomes dependent on N. More specifically, in Fig. 9, curves with different sizes separate at $T/t \approx 0.05$, the temperature at which the correlation length ξ becomes comparable to the linear lattice size. The temperature, which is set by the effective exchange coupling J_{eff}, where $\xi(T) \sim L$ decreases for larger V/t (not shown). As a consequence, simulations for this parameter regime has become a challenging issue for DQMC. The dependence of J_{eff} on V has been estimated within perturbation theory[37].

The order parameter is obtained by carrying out a finite-size scaling analysis of the spin structure factor. The saturated (large β) values of $S(0)$, for different lattice
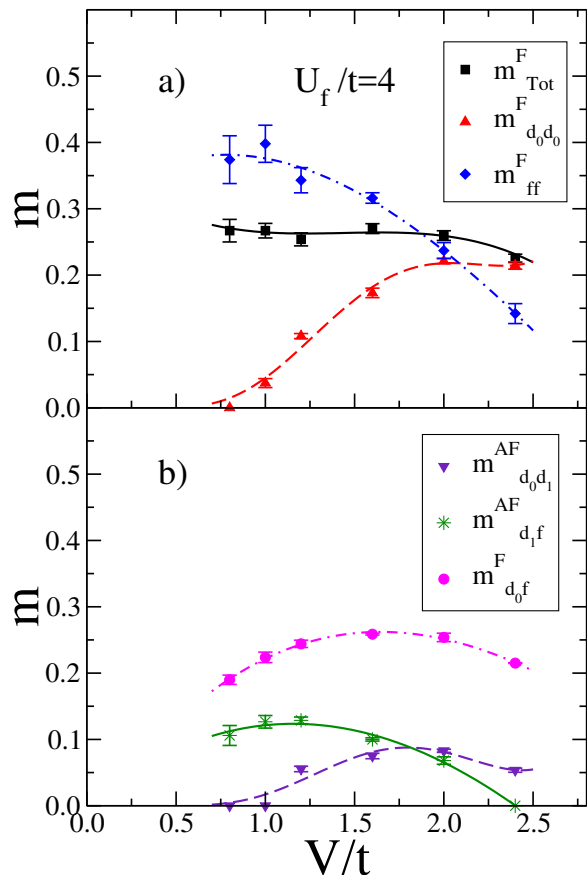
FIG. 11: (a) The order parameter m_{tot}^F and its individual contributions $m_{d_0 d_0}^F$ and m_{ff}^F as well as (b) $m_{d_0 d_1}^{AF}$, $m_{d_1 f}^{AF}$ and $m_{d_0 f}^F$ as functions of V/t. $m_{d_1 d_1}^F$ is zero for all values of V/t. The curves are guides to the eye.

sizes are fit to a linear spin-wave scaling[73],

$$\frac{S(0)}{N_{cell}} = m_{tot}^2 + \frac{a}{\sqrt{N_{cell}}},\qquad (12)$$

with m_{tot}^2 being the extrapolated global ferromagnetic order parameter; see Fig. 10. This result confirms the existence of long range ferromagnetism in the ground state, even for V/t more than twice $V_c/t \sim 1$ where the system becomes a spin liquid in the undepleted case. Fig. 11 (a) presents the behavior of m_{tot} (squares; black solid line) as a function of V/t. Interestingly, the ferromagnetic order parameter is almost independent of the hybridization over the range shown.

The analysis of the short range spin correlations for different orbitals in Figs. 7 and 8 already provided some insight into where magnetism "lives". Then, we proceed by investigating the individual contributions to magnetism, by means of Eq. (11). However, as discussed above, the correlation functions of d_0-d_1 and d_1-f sites are always negative, thus we define $S_{\alpha\gamma}^{AF} = -S_{\alpha\gamma}$ for these pairs of sites; this corresponds to taking their antiferromagnetic contribution. By the same token, we define $S_{\alpha\gamma}^F = S_{\alpha\gamma}$ for those pairs of sites in which their

correlation funtions are always ferromagnetic. As with the global structure factor, we perform a linear scaling for each channel[81], i.e. $S_{\alpha\gamma}^{F(AF)}/N_{cells} \to \left(m_{\alpha\gamma}^{F(AF)}\right)^2$, when $1/\sqrt{N_{cells}} \to 0$. These extrapolated values are displayed in Fig. 11. We omit $m_{d_1 d_1}^F$, which is small for the entire range of V/t examined.

As shown in Fig. 11 (a), at small hybridization the largest contribution to the total magnetism comes from the f-sites, while $m_{d_0 d_0}^F$ is negligible. However, as V/t increases, a crossover between f and d_0-site contributions takes place, with the suppression of the former and the enhancement of the latter, while the total magnetism is kept constant. The contributions from different channels are exhibited in Figure 11 (b), with $m_{d_0 f}^{AF}$ being the largest over the entire range of V/t we analyzed. This should not be surprising for small hybridization (i.e. $V/t < 1$), since RKKY leads to long-range spin correlations between d and f orbitals. However, these strong spin correlations even for large V/t (> 1) are the key for supporting the formation of a magnetic ground state. In this region, attempts to screen the f-electrons reduce their contribution to magnetism, but, owing to the large antiferromagnetic correlation between d_0 and f-sites, the localized d_0-electrons can indirectly interact with each other, leading to long range order in their sublattice. The same assumption can be inferred from $m_{d_0 d_1}^{AF}$. A similar crossover (from f to d_0 magnetism) is observed in a single spin depleted KLM in a one-dimensional chain[55], as well as in higher dimensions within dynamical mean-field theory (DMFT)[36,38]. Unlike DMFT, the DQMC approach includes nonlocal correlations thus providing additional insight into the crossover.

Interestingly, the order parameter on conduction electron sites without an f partner, $m_{d_0 d_0}^F$, becomes non-negligible at $V_c/t \approx 1$, the value of the QCP for the undepleted PAM, for $U_f/t = 4$.[7,10] In this situation V_c/t is the characteristic energy scale to form singlets, whose formation is prevented on the depleted lattice by the presence of unpaired d-electrons. One should notice that, not coincidentally, the AF $m_{d_0 d_1}^{AF}$ contribution to magnetism starts being relevant at V_c/t as well. As discussed above, since d_0-d_0 spin correlations are also mediated by d_1 sites, one thus expects long range spin correlations in the d_0-d_1 channel in order for $m_{d_0 d_0}^F$ be non-negligible. On the other hand, for large hybridization, namely $V/t \gtrsim 1$, $m_{d_1 f}^{AF}$ is suppressed, i.e. d_1-f spin correlations start becoming short ranged, as a symptom of the attempts to form singlets. These results strongly suggest that, despite the fact that magnetism remains present, there is a "memory" of the undepleted PAM QCP. In other words, the d_0 electrons start being localized and, therefore, interacting with each other when hybridization is larger than the energy scale for the formation of singlets in the undepleted PAM. Thus, this crossover will change its position according to the $V_c(U_f)$.[82] Finally, we should mention that the results for the dynamical quantities in the single depletion case (see
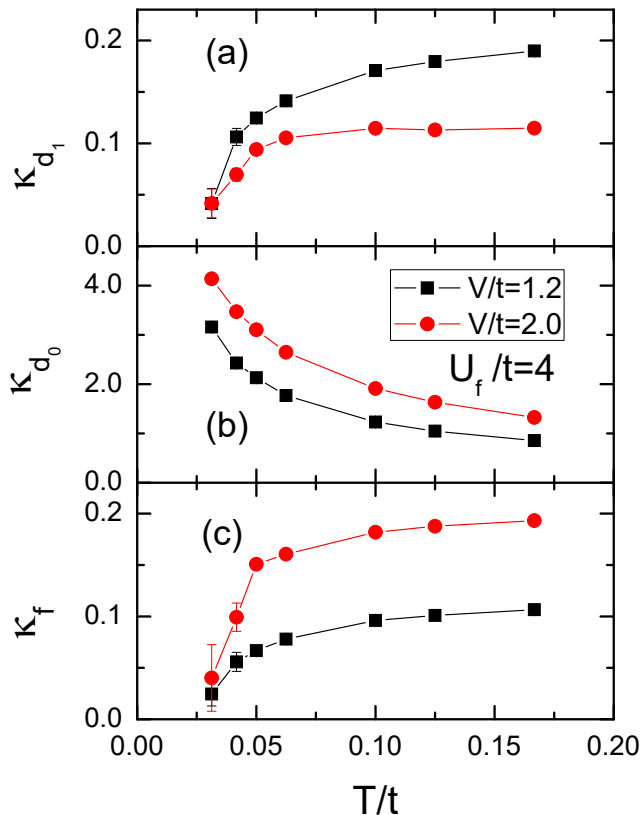
FIG. 12: The orbital resolved compressibilities as functions of T/t at (a) d_1-, (b) d_0- and (c) f-sites. On the f-sites where U_f is non-zero, and the conduction sites d_1 to which they are hybridized by V, the compressibility vanishes as $T \to 0$. However on the d_0-sites where only the conduction orbital remains following depletion, κ remains large at low T.

the previous section) give further insights into the nature of this long-ranged ferrimagnetic state: as the number of d_0-sites (or impurities) increases, the broken singlets around them may form larger clusters, hence leading to long ranged spin correlations; the localized electrons on d_0-sites behave similarly to spins with a small magnetic moment (due to $U_d = 0$), but also contributing to magnetism.

V. TRANSPORT PROPERTIES

We conclude with a discussion of transport properties. We first examine the electronic compressibilities for each individual orbital κ_α, which exhibit an interesting behavior (Fig. 12). κ_{d_1} and κ_f, the compressibilities on the two sites connected by V, fall as the temperature is lowered for both $V/t = 1.2$ and $V/t = 2.0$. On the other hand, the d_0-site compressibility κ_{d_0} is much larger, and grows as T/t decreases. Such feature of d_0-sites is deeply connected with the formation of localized electronic states on them, as discussed in Sec. III. Thus,
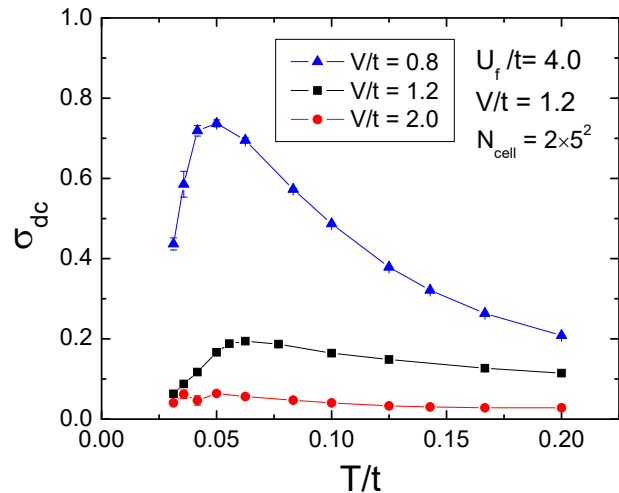

FIG. 13: Conductivity σ_{dc} as a function of temperature T at $V/t = 0.8$, 1.2 and 2.0. σ_{dc} turns sharply downward at the same temperature $T \sim 0.05t$ where the compressibility on the d_1 and d_0 sites also decreases more rapidly (Fig. 12) and the ferromagnetic structure factor signals the beginning of large spin correlation lengths (Fig. 9).

one should expect a large density of states at the Fermi level due to the absence of local repulsion on d_0-sites, but with these available states belonging to them.

Although the system is compressible, as evidenced by the data in Fig. 12, it is an insulator. The metallicity of a system should be determined not only by the available states at Fermi level, but also by its current-current correlation functions and, ultimately, by its conductivity, Eq. (6). As displayed in Fig. 13, the temperature dependence of the conductivity σ_{dc} indicates an insulating behavior. This is similar to what happens for the single band Hubbard model on a square lattice, where σ_{dc} also vanishes for the entire range of U/t, as the system crosses over from a Slater to a Mott insulator; the same also occurs for the entire range of V/t for the undepleted PAM, whose QCP separates an AF insulator from a singlet phase with a hybridization gap. However, here the emergence of this insulating state is related to the lack of available states on nearest-neighbor d_0-sites, due to the tendency of d_1-f singlet formation. That is, although one can accommodate new electrons on d_0-sites, their hopping throughout the lattice is hindered. We believe this behavior is generic to the depleted PAM as well: despite being compressible, the entire phase diagram at half filled corresponds to an insulating system.

It is worth mentioning that a compressible insulator (or a *gapless* insulator) has already been predicted to occur in other systems, such as in one-dimensional Hubbard superlattices.[74] In this case, a periodic arrangement of L_1 noninteracting sites and L_2 interacting sites leads to a compressible insulator ground state, since one can add charge in the noninteracting sites without energy cost. By the same token, $U_d = 0$ in the depleted PAM, which

in addition to the large local density of states on the d_0-sites, allows one to accomodate a second electron on them, creating a compressible (insulator) state.

VI. CONCLUSIONS

In this paper we have studied the properties of a two-dimensional periodic Anderson model with (i) a single localized f-site depletion and (ii) one half of the f-sites regularly removed. In the former case, by examining the behavior of the local magnetic susceptibility, we noticed an enhancement of spin-spin correlations, with the creation of an antiferromagnetic 'cloud' around the defect. This enhancement occurs due to the break-up of singlets around the impurity, owing to the exchange interaction between the localized f-electrons and the unpaired d-electron. We have also investigated spectral properties, such as the local density of states. We observed that a single depletion creates a large sprectral weight at the Fermi level on the unpaired d-site, corresponding to a localized state on it.

The latter case, i.e. the one half f-sites depletion, leads to some unique properties. First, it has long-range ferrimagnetic order, consistent with Tsunetsugu's theorem[67] for the KLM (and ultimately to Lieb's theorem[25] for the Hubbard Hamiltonian) concerning the total spin in the ground state of a bipartite lattice with unequal numbers of sublattice sites. Analyses of the spin correlations in different channels indicate that at small f-d hybridization, V, the magnetic order is dominated by the remaining f-sites, but at large V there is a crossover: the magnetic order becomes strongly driven by those conduction sites which have lost their local orbital partners. It is a remarkable instance of magnetism from noninteracting orbitals (U_d=0). Overall, although the total ferromagnetic order parameter is surprisingly constant, its individual channel contributions provide evidence that the crossover between f and d magnetism occurs at the AF-singlet QCP of the undepleted PAM.

The emergence of this ferromagnetic state can be understood via a strong coupling (i.e. $U, V \gg t$) analysis, as discussed in Ref. 37. With the aid of fourth-order perturbation theory, the system can be mapped onto a Heisenberg-like Hamiltonian, in which the localized electrons on d_0-sites interact with each other mediated by intervening d_1-f singlets, leading to a ferromagnetic effective exchange coupling [of typical magnitude $J_{\text{eff}} \sim t^4(U^3 + 48UV^2)/24V^6$].

Two additional features stand out in the transport properties. First, the system is compressible at half-filling. This cannot be attributed simply to the presence of conduction sites at which $U_d = 0$, since these are present in the undepleted PAM, for which $\kappa = 0$. Thus $\kappa \neq 0$ must be attributed to the depletion and, in particular, to the mismatch of conduction and local spin orbitals which prevents all sites from participating in singlet formation. Related issues have been raised in the reversed situation where the number of local orbitals exceeds the number of conduction electrons available for screening[75,76]. Second, despite this non-vanishing compressibility, the system is insulating; the conductivity σ_{dc} goes to zero as the temperature is lowered.

Phases where insulating behavior and nonzero compressibility are partnered together constitute a prominent feature of the physics of the *boson* Hubbard model[77]. There, the introduction of disorder results in a new 'Bose-glass' phase, which has zero superfluid density, like the Mott insulator (MI) of the clean model, but which is compressible, unlike the MI[78]. In the depleted PAM studied here we have demonstrated a fermionic analog, a phase which is insulating like the original AF and singlet regimes of the undepleted PAM, but has nonzero κ. This compressible ferrimagnet originates from depletion rather than from disorder.

[1] F. Gebbhard, *The Mott Metal-Insulator Transition: Models and Methods* (Springer-Verlag, New York, 1997).

[2] P. Fazekas, *Lecture notes on electron correlation and magnetism*, vol. 5 (World scientific, 1999).

[3] J. E. Hirsch, Phys. Rev. B **31**, 4403 (1985), URL https://link.aps.org/doi/10.1103/PhysRevB.31.4403.

[4] J. E. Hirsch and S. Tang, Phys. Rev. Lett. **62**, 591 (1989), URL https://link.aps.org/doi/10.1103/PhysRevLett.62.591.

[5] Y. Nagaoka, Phys. Rev. **147**, 392 (1966), URL https://link.aps.org/doi/10.1103/PhysRev.147.392.

[6] H. Tasaki, Prog. Theor. Phys. **99**, 489 (1998), URL https://doi.org/10.1143/PTP.99.489.

[7] M. Vekić, J. W. Cannon, D. J. Scalapino, R. T. Scalettar, and R. L. Sugar, Phys. Rev. Lett. **74**, 2367 (1995), URL http://link.aps.org/doi/10.1103/PhysRevLett.74.2367.

[8] G. R. Stewart, Rev. Mod. Phys. **73**, 797 (2001), URL https://link.aps.org/doi/10.1103/RevModPhys.73.797.

[9] L. De Leo, M. Civelli, and G. Kotliar, Phys. Rev. Lett. **101**, 256404 (2008), URL https://link.aps.org/doi/10.1103/PhysRevLett.101.256404.

[10] W. Hu, R. T. Scalettar, E. W. Huang, and B. Moritz, Phys. Rev. B **95**, 235122 (2017), URL https://link.aps.org/doi/10.1103/PhysRevB.95.235122.

[11] A. Cameron, G. Friemel, and D. Inosov, Reports on Progress in Physics **79**, 066502 (2016).

[12] D. Scalapino, Proceedings of the International School of Physics, R.A. Broglia and J. R. Schrieffer, eds (North-Holland, New York, and references cited therein. (1994).

[13] S. Zhang, J. Carlson, and J. E. Gubernatis, Phys. Rev. Lett. **78**, 4486 (1997), URL https://link.aps.org/doi/10.1103/PhysRevLett.78.4486.

[14] A. Millis, Nature **392**, 438 (1998).

[15] T. Maier, M. Jarrell, T. Pruschke, and J. Keller, Phys. Rev. Lett. **85**, 1524 (2000), URL https://link.aps.org/doi/10.1103/PhysRevLett.85.1524.

[16] M. Capone and G. Kotliar, Journal of Magnetism and Magnetic Materials **310**, 529 (2007), ISSN 0304-8853, proceedings of the 17th International Conference on Magnetism, URL http://www.sciencedirect.com/science/article/pii/S0304885306013126.

[17] W. Wu and A.-M.-S. Tremblay, Phys. Rev. X **5**, 011019 (2015), URL https://link.aps.org/doi/10.1103/PhysRevX.5.011019.

[18] G. R. Stewart, Rev. Mod. Phys. **56**, 755 (1984), URL https://link.aps.org/doi/10.1103/RevModPhys.56.755.

[19] J. E. Hirsch and R. M. Fye, Phys. Rev. Lett. **56**, 2521 (1986), URL https://link.aps.org/doi/10.1103/PhysRevLett.56.2521.

[20] R. M. Fye, Phys. Rev. B **41**, 2490 (1990), URL https://link.aps.org/doi/10.1103/PhysRevB.41.2490.

[21] R. M. Fye and D. J. Scalapino, Phys. Rev. B **44**, 7486 (1991), URL https://link.aps.org/doi/10.1103/PhysRevB.44.7486.

[22] T. Costi, E. Müller-Hartmann, and K. Ulrich, Solid State Communications **66**, 343 (1988), ISSN 0038-1098, URL http://www.sciencedirect.com/science/article/pii/0038109888908538.

[23] E. Dagotto, T. Hotta, and A. Moreo, Physics Reports **344**, 1 (2001), URL http://www.sciencedirect.com/science/article/pii/S0370157300001216.

[24] Q. Si, R. Yu, and E. Abrahams, Nature Rev. Mat. **1**, 16017 (2016).

[25] E. H. Lieb, Phys. Rev. Lett. **62**, 1201 (1989), URL http://link.aps.org/doi/10.1103/PhysRevLett.62.1201.

[26] M. Troyer, H. Kontani, and K. Ueda, Phys. Rev. Lett. **76**, 3822 (1996), URL https://link.aps.org/doi/10.1103/PhysRevLett.76.3822.

[27] E. Khatami, R. R. P. Singh, W. E. Pickett, and R. T. Scalettar, Phys. Rev. Lett. **113**, 106402 (2014), URL https://link.aps.org/doi/10.1103/PhysRevLett.113.106402.

[28] H.-M. Guo, T. Mendes-Santos, W. E. Pickett, and R. T. Scalettar, Phys. Rev. B **95**, 045131 (2017), URL https://link.aps.org/doi/10.1103/PhysRevB.95.045131.

[29] A. S. Botana, V. Pardo, W. E. Pickett, and M. R. Norman, Phys. Rev. B **94**, 081105 (2016), URL https://link.aps.org/doi/10.1103/PhysRevB.94.081105.

[30] J. Zhang, Y.-S. Chen, D. Phelan, H. Zheng, M. Norman, and J. Mitchell, Proceedings of the National Academy of Sciences of the United States of America **113**, 8945 (2016).

[31] G. Xiao, M. Z. Cieplak, A. Gavrin, F. H. Streitz, A. Bakhshai, and C. L. Chien, Phys. Rev. Lett. **60**, 1446 (1988), URL https://link.aps.org/doi/10.1103/PhysRevLett.60.1446.

[32] B. Keimer, A. Aharony, A. Auerbach, R. J. Birgeneau, A. Cassanho, Y. Endoh, R. W. Erwin, M. A. Kastner, and G. Shirane, Phys. Rev. B **45**, 7430 (1992), URL https://link.aps.org/doi/10.1103/PhysRevB.45.7430.

[33] A. V. Mahajan, H. Alloul, G. Collin, and J. F. Marucco, Phys. Rev. Lett. **72**, 3100 (1994), URL https://link.aps.org/doi/10.1103/PhysRevLett.72.3100.

[34] M.-H. Julien, T. Fehér, M. Horvatić, C. Berthier, O. N. Bakharev, P. Ségransan, G. Collin, and J.-F. Marucco, Phys. Rev. Lett. **84**, 3422 (2000), URL https://link.aps.org/doi/10.1103/PhysRevLett.84.3422.

[35] B. Coles, S. Oseroff, and Z. Fisk, Journal of Physics F: Metal Physics **17**, L169 (1987), URL http://stacks.iop.org/0305-4608/17/i=8/a=006.

[36] I. Titvinidze, A. Schwabe, and M. Potthoff, Phys. Rev. B **90**, 045112 (2014), URL http://link.aps.org/doi/10.1103/PhysRevB.90.045112.

[37] I. Titvinidze, A. Schwabe, and M. Potthoff, Eur. Phys. J. B **88**, 9 (2015), URL http://dx.doi.org/10.1140/epjb/e2014-50772-1.

[38] M. W. Aulbach, I. Titvinidze, and M. Potthoff, Phys. Rev. B **91**, 174420 (2015), URL http://link.aps.org/doi/10.1103/PhysRevB.91.174420.

[39] K. Seki, T. Shirakawa, Q. Zhang, T. Li, and S. Yunoki, Phys. Rev. B **93**, 155419 (2016), URL https://link.aps.org/doi/10.1103/PhysRevB.93.155419.

[40] F. F. Assaad, Phys. Rev. B **65**, 115104 (2002), URL https://link.aps.org/doi/10.1103/PhysRevB.65.115104.

[41] R. Blankenbecler, D. J. Scalapino, and R. L. Sugar, Phys. Rev. D **24**, 2278 (1981), URL https://link.aps.org/doi/10.1103/PhysRevD.24.2278.

[42] R. R. dos Santos, Brazilian Journal of Physics **33**, 36 (2003), ISSN 0103-9733, URL http://www.scielo.br/scielo.php?script=sci_arttext&pid=S0103-97332003000100003&nrm=iso.

[43] Z.-X. Li, Y.-F. Jiang, and H. Yao, Phys. Rev. Lett. **117**, 267002 (2016), URL https://link.aps.org/doi/10.1103/PhysRevLett.117.267002.

[44] E. Y. Loh, J. E. Gubernatis, R. T. Scalettar, S. R. White, D. J. Scalapino, and R. L. Sugar, Phys. Rev. B **41**, 9301 (1990), URL https://link.aps.org/doi/10.1103/PhysRevB.41.9301.

[45] M. Troyer and U.-J. Wiese, Phys. Rev. Lett. **94**, 170201 (2005), URL https://link.aps.org/doi/10.1103/PhysRevLett.94.170201.

[46] N. Trivedi, R. T. Scalettar, and M. Randeria, Phys. Rev. B **54**, R3756 (1996), URL http://link.aps.org/doi/10.1103/PhysRevB.54.R3756.

[47] P. J. H. Denteneer, R. T. Scalettar, and N. Trivedi, Phys. Rev. Lett. **83**, 4610 (1999), URL http://link.aps.org/doi/10.1103/PhysRevLett.83.4610.

[48] R. R. Urbano, B.-L. Young, N. J. Curro, J. D. Thompson, L. D. Pham, and Z. Fisk, Phys. Rev. Lett. **99**, 146402 (2007), URL http://link.aps.org/doi/10.1103/PhysRevLett.99.146402.

[49] S. Seo, X. Lu, J.-X. Zhu, R. R. Urbano, N. Curro, E. D. Bauer, V. A. Sidorov, L. D. Pham, T. Park, Z. Fisk, et al., Nat Phys **10**, 120 (2014), URL http://dx.doi.org/10.1038/nphys2820.

[50] H. Sakai, F. Ronning, J.-X. Zhu, N. Wakeham, H. Yasuoka, Y. Tokunaga, S. Kambe, E. D. Bauer, and J. D. Thompson, Phys. Rev. B **92**, 121105 (2015), URL https://link.aps.org/doi/10.1103/PhysRevB.92.121105.

[51] K. Chen, F. Strigari, M. Sundermann, Z. Hu, Z. Fisk, E. D. Bauer, P. F. S. Rosa, J. L. Sarrao, J. D. Thompson, J. Herrero-Martin, et al., Phys. Rev. B **97**, 045134 (2018), URL https://link.aps.org/doi/10.1103/PhysRevB.97.045134.

[52] A. P. Dioguardi, T. Kissikov, C. H. Lin, K. R. Shirer, M. M. Lawson, H.-J. Grafe, J.-H. Chu, I. R. Fisher, R. M. Fernandes, and N. J. Curro, Phys. Rev. Lett. **116**, 107202 (2016), URL https://link.aps.org/doi/10.1103/PhysRevLett.116.107202.

[53] A. Benali, Z. J. Bai, N. J. Curro, and R. T. Scalettar, Phys. Rev. B **94**, 085132 (2016), URL http://link.aps.org/doi/10.1103/PhysRevB.94.085132.

[54] T. Mendes-Santos, N. C. Costa, G. Batrouni, N. Curro, R. R. dos Santos, T. Paiva, and R. T. Scalettar, Phys. Rev. B **95**, 054419 (2017), URL http://link.aps.org/doi/10.1103/PhysRevB.95.054419.

[55] C. C. Yu, Phys. Rev. B **54**, 15917 (1996), URL http://link.aps.org/doi/10.1103/PhysRevB.54.15917.

[56] M. C. Martin, M. Hase, K. Hirota, G. Shirane, Y. Sasago, N. Koide, and K. Uchinokura, Phys. Rev. B **56**, 3173 (1997), URL https://link.aps.org/doi/10.1103/PhysRevB.56.3173.

[57] M. Azuma, Y. Fujishiro, M. Takano, M. Nohara, and H. Takagi, Phys. Rev. B **55**, R8658 (1997), URL https://link.aps.org/doi/10.1103/PhysRevB.55.R8658.

[58] J. Figgins and D. K. Morr, Phys. Rev. Lett. **107**, 066401 (2011), URL https://link.aps.org/doi/10.1103/PhysRevLett.107.066401.

[59] N. Trivedi and M. Randeria, Phys. Rev. Lett. **75**, 312 (1995), URL http://link.aps.org/doi/10.1103/PhysRevLett.75.312.

[60] M. Jarrell and J. Gubernatis, Phys. Rep. **269**, 133 (1996), ISSN 0370-1573, URL http://www.sciencedirect.com/science/article/pii/0370157395000747.

[61] R. Sollie and P. Schlottmann, J. of App. Phys. **69**, 5478 (1991), URL http://scitation.aip.org/content/aip/journal/jap/69/8/10.1063/1.347971.

[62] R. Sollie and P. Schlottmann, J. of App. Phys. **70**, 5803 (1991), URL http://scitation.aip.org/content/aip/journal/jap/70/10/10.1063/1.350142.

[63] K. H. Höglund, A. W. Sandvik, and S. Sachdev, Phys. Rev. Lett. **98**, 087203 (2007), URL https://link.aps.org/doi/10.1103/PhysRevLett.98.087203.

[64] J. Bobroff, N. Laflorencie, L. K. Alexander, A. V. Mahajan, B. Koteswararao, and P. Mendels, Phys. Rev. Lett. **103**, 047201 (2009), URL https://link.aps.org/doi/10.1103/PhysRevLett.103.047201.

[65] P. Schlottmann, Phys. Rev. B **54**, 12324 (1996), URL http://link.aps.org/doi/10.1103/PhysRevB.54.12324.

[66] S. Doniach and P. Fazekas, Philosophical Magazine Part B **65**, 1171 (1992), URL http://dx.doi.org/10.1080/13642819208215081.

[67] H. Tsunetsugu, Phys. Rev. B **55**, 3042 (1997), URL http://link.aps.org/doi/10.1103/PhysRevB.55.3042.

[68] E. H. Lieb, Phys. Rev. Lett. **62**, 1927 (1989), URL http://link.aps.org/doi/10.1103/PhysRevLett.62.1927.5.

[69] N. C. Costa, T. Mendes-Santos, T. Paiva, R. R. dos Santos, and R. T. Scalettar, Phys. Rev. B **94**, 155107 (2016), URL http://link.aps.org/doi/10.1103/PhysRevB.94.155107.

[70] D. Vollhardt, N. Blümer, K. Held, and M. Kollar, *Band-Ferromagnetism: Ground-State and Finite-Temperature Phenomena* (Springer Berlin Heidelberg, Berlin, Heidelberg, 2001), chap. Metallic Ferromagnetism — An Electronic Correlation Phenomenon, pp. 191–207, URL http://dx.doi.org/10.1007/3-540-44610-9_13.

[71] R. Mondaini and T. Paiva, Phys. Rev. B **95**, 075142 (2017), URL http://link.aps.org/doi/10.1103/PhysRevB.95.075142.

[72] S.-Q. Shen, Phys. Rev. B **53**, 14252 (1996), URL http://link.aps.org/doi/10.1103/PhysRevB.53.14252.

[73] D. A. Huse, Phys. Rev. B **37**, 2380 (1988), URL http://link.aps.org/doi/10.1103/PhysRevB.37.2380.

[74] J. Silva-Valencia, E. Miranda, and R. R. dos Santos, Phys. Rev. B **65**, 115115 (2002), URL https://link.aps.org/doi/10.1103/PhysRevB.65.115115.

[75] N. S. Vidhyadhiraja, A. N. Tahvildar-Zadeh, M. Jarrell, and H. R. Krishnamurthy, Europhys. Lett. **49**, 459 (2000), URL http://stacks.iop.org/0295-5075/49/i=4/a=459.

[76] D. Meyer and W. Nolting, Phys. Rev. B **61**, 13465 (2000), URL https://link.aps.org/doi/10.1103/PhysRevB.61.13465.

[77] M. P. A. Fisher, P. B. Weichman, G. Grinstein, and D. S. Fisher, Phys. Rev. B **40**, 546 (1989), URL https://link.aps.org/doi/10.1103/PhysRevB.40.546.

[78] R. T. Scalettar, G. G. Batrouni, and G. T. Zimanyi, Phys. Rev. Lett. **66**, 3144 (1991), URL https://link.aps.org/doi/10.1103/PhysRevLett.66.3144.

[79] The In electronic configuration is [Kr] $5s^2\,4d^{10}$, while that of Cd is [Kr] $5s^2\,4d^{10}\,5p^1$.

[80] This kind of depletion may be connected with La-doped heavy fermion materials, such as $Ce_{1-x}La_xCoIn_5$. Since the electronic configuration of Ce is [Xe] $6s^2\,4f^1\,5d^1$, while the La configuration is [Xe] $6s^2\,5d^1$, the main effect of La doping is to remove a localized f-electron. Nonetheless, there is no experimental evidence of magnetic enhancement for La substitution in $CeCoIn_5$.

[81] The individual contributions $S_{\alpha\gamma}$ of channels $\{\alpha\gamma\}=\{d_0d_1\}$, $\{d_0f\}$ and $\{d_1f\}$ are divided by two before we perform the scaling. It assures a site normalized order parameter for all individual contributions.

[82] Ref. 10 presents an accurate determination of the undepleted PAM QCPs, $V_c(U_f)$.